Received: 4 February 2022 | Revised: 6 April 2022 | Accepted: 17 June 2022

IET Generation, Transmission & Distribution

DOI: 10.1049/gtd2.12546

The Institution of Engineering and Technology WILEY

ORIGINAL RESEARCH

Novel non-linear control of DFIG and UPFC for transient stability increment of power system

Sadegh Ghaedi | **Saeed Abazari** | **Gholamreza Arab Markadeh**

Faculty of Engineering, Shahrekord University, Shahrekord, Iran

Correspondence
Saeed Abazari, Faculty of Engineering, Shahrekord University, Shahrekord, Iran.
Email: abazari-s@eng.sku.ac.ir

Abstract

This paper offers novel non-linear control of a doubly fed induction generator (DFIG) and unified power flow controller (UPFC) for transient stability increment with transient energy function (TEF) and sliding mode observer in a power system. First, the TEF technique is considered for the damping control in a power system with a synchronous generator (SG), DFIG, and UPFC, and then the controller time-derivative signals are estimated by a second-order sliding mode observer. The importance of the issue is in the employ of a complete UPFC model. Also, a one-axis model is used for DFIG that is similar to the SG model. Another characteristic of the novel non-linear technique is robust versus system topology changes and variable time delay of the control signals. To evaluate the performance of the novel non-linear control method for increment transient stability, simulation studies are performed on a two-machine connected to an infinite bus (TMIB), the IEEE 9-bus, and the New England Standard 39-bus power system. The results determine that the novel non-linear control method decreases the first swing of fluctuations admissibly and enhancement stability margins considerably.

1 | INTRODUCTION

With the expansion of the power network, its stability is of more significance in the performance of the power systems. Also, the new transmission networks are increasingly pressured with increasing daily demands and restrictions on the construction of new lines. On the other hand, the market for renewable generating sources is enhancing every day due to the environmental pollution factors and the energy crisis that has affected the world. Among renewable sources, wind energy has a significant contribution to the production of electricity [1]. Lately, power system performance has faced the difficulty of preservation stability when disturbances happen in the power system, containing the variation presented with renewable energy sources and the merge of wind power in conventional power networks. Transient stability is mostly affected by the types of generators in the power system, and the DFIG dynamic properties are distinct from SG. Therefore, the analysis of the transient stability of DFIG and SG in power systems has become a very significant subject [2].

The other one method that can help to decrease pressure and the problem of preservation stability is the use of Flexible AC Transmission System (FACTS) devices [3]. Among various FACTS devices, the UPFC offers the most comprehensive and complete method in this field. By installing a UPFC in the transmission system, the margin of stability increases, and as a result the power transfer and the thermal limitation of the line conductors increase [4]. Also, UPFC can prepare technical solutions to increase the efficiency of merged wind power systems in conventional [5].

A power system stabilizer (PSS) is a common technique for system fluctuations damping and the recent development in enforcement FACTS has reduced the damping of these fluctuations [6, 7]. Also In the issue of multi-objective optimization [8], the coordinated scheme between UPFC and PSS to increase the damping of the electromechanical modes is studied in [9].

A transient stability enhancement in a power system with UPFC has been investigated by POD and PID controllers [10]. In [11], the Control Lyapunov Function (CLF) and Power Oscillation Damping (POD) are utilized to dampen the fluctuations.

The POD controller of the UPFC is proposed for damping fluctuations due to disturbances in an aggregated wind farm [12].

With regards to recent advances in non-linear controllers, various strategies, containing TEF analytical methods [13], have been utilized to model FACTS devices for damping fluctuations [14, 15]. In [16], the term TEF was coined to denote the transient energy function of a multi-machine power system with UPFC. The TEF method with Lyapunov's direct method can provide the desired damping of fluctuations to enhance transient stability [17].

A new challenging issue has emerged in the definition of TEF for power systems with aggregated wind farms and FACTS devices [18, 19]. In [20], the effect of aggregated wind farms using DFIG on the power system stability is investigated. A third-order model is obtained for a DFIG that is similar to the standard one-axis model of SG. In [21], the transient stability problem of a DFIG was addressed, for example, how the main DFIG parameters affect it. A system energy function is modeled based on an optimal control technique for output stabilization of DFIG to maintain the network power that is isolated from wind power output oscillations [22]. An adaptive sliding mode control technique to a power system with UPFC is proposed to increase the transient stability of a multi-machine power system with DFIG that uses the power components [23]. A non-linear control technique has been proposed to increase the transient stability in the power systems with SG, DFIG, and STATCOM [24].

A unified design of neural networks and TEF to model the supernumerary damping control in the power system with UPFC for damping of fluctuations is provided in [25] and [26]. In [27], the ability of the adaptive neuro-fuzzy inference system to estimate the best UPFC control values to increase the efficiency of a DFIG during fault is investigated. The non-linear controller linearization feedback as a proper controller is provided to improve various parameters, which changes the control input so that FACTS devices can behave linearly under entire dynamics of non-linear that occur in the power system [28].

A practicable technique is provided to specify multiple-parameter control in a power system to improve stability [29] which by using the TEF method achieves a global optimum in Lyapunov's concept. Also, in [30] and [31], a control technique based on Lyapunov theory by utilizing a controllable series capacitor by a proper control strategy is provided to increase the additional oscillations damping of the power system. The time-derivative of control laws is obtained via band-pass filters which in this case noise problem is not completely solved.

The proposed control design presents various supremacies. More of the suggested techniques are based on linearized system techniques such as PSS which responses under severe disturbances could not be completely acquired. The other non-linear control techniques, for example, feedback linearization changes the basic system to a normal system. In return, the suggested design is a non-linear control technique that presents enhanced degrees of freedom in the scheme through the choice of a proper transient energy function. Also in non-linear control design techniques, due to the presence of noise, the time-derivative of control laws cannot be reached directly by numerical differentiation. By using a novel non-linear TEF controller for DFIG and UPFC that estimates the parameters with the second sliding mode observer, can solve these problems and assist in damping of oscillations.

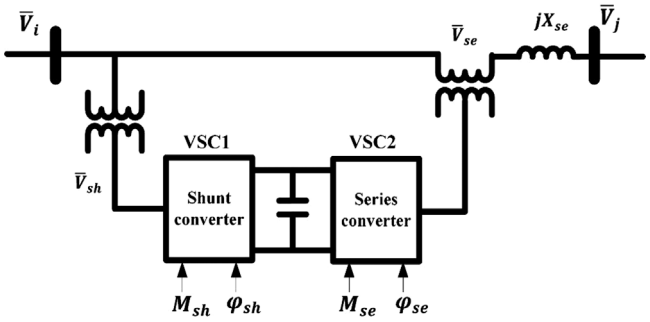

FIGURE 1 The scheme of a UPFC

In this study, non-linear control of DFIG and UPFC for transient stability increment of the power system is comprehensively performed. The contributions of the paper include the use of the following two at the same time.

1. The proposed control rules are achieved with two DFIG control variables and four UPFC control variables by interaction with each other.
2. The time-derivative signals of the UPFC and DFIG controllers are estimated according to a second sliding mode observer.

The paper is arranged as follows. Section 2 presents the modeling of the UPFC. The multi-machine power system model will be developed in Section 3. In Section 4, novel non-linear control design will be introduced. In Section 5, simulation design will approve the performance of the novel proposed control strategy. Conclusions are presented in Section 6.

2 | MODELING OF THE UPFC

A scheme of the UPFC is shown in Figure 1 [3]. A UPFC consists of a series controller (SSSC) and a shunt controller (STATCOM) and series and shunt converters apply a Voltage Sourced Converter (VSC).

The UPFC acts by using the injection of voltage sources $\bar{V}_{se}$ and $\bar{V}_{sh}$ by modifiable magnitude and angle. The controllable voltage $\bar{V}_{se}$ and $\bar{V}_{sh}$ in converters are obtained as follows:

$$\bar{V}_{se} = M_{se}\, V_c\, e^{J(\theta_i+\varphi_{se})} = \left(U_{sed} + JU_{seq}\right)\, e^{J\theta_i}, \tag{1.a}$$

$$\bar{V}_{sh} = M_{sh}\, V_c\, e^{J(\theta_i+\varphi_{sh})} = \left(U_{shd} + JU_{shq}\right)\, e^{J\theta_i}, \tag{1.b}$$

where V_c represents the DC side voltage of UPFC.

2.1 | Power flow modeling

The UPFC can be demonstrated in the form of a power flow model [32]. When the UPFC is placed betwixt buses i and j, the power flow of UPFC can be obtained as follows:

$$\begin{cases} P_{ui} = B_{se}\, V_i V_{seq} + B_{sh} V_i V_{sbq} \\ Q_{ui} = B_{se}\, V_i V_{sed} + B_{sh} V_i V_{sbd} \\ P_{uj} = -B_{se} V_j V_{sed} \sin\left(\theta_{ij}\right) - B_{se} V_j V_{seq} \cos\left(\theta_{ij}\right) \\ Q_{uj} = -B_{se} V_j V_{sed} \cos\left(\theta_{ij}\right) + B_{se} V_j V_{seq} \sin\left(\theta_{ij}\right) \end{cases}. \quad (2)$$

3 | MULTI-MACHINE POWER SYSTEM MODEL

Consider the power network with $m + l + n$ nodes that contains m-SG and l-DFIG and n load buses that are modeled as constant impedances. The voltage phasor of the internal generator bus is $E_i' \angle \delta_i$ and that of the external generator bus is $V_i \angle \theta_i$. Dynamic models of this power system including SGs and DFIGs can be as follows.

3.1 | SG modeling

The dynamics of any generator will be expressed in the form of the COI reference frame. The COI to all δ_{COI} and the center of speed ω_{COI} are determined as follows [33]

$$\delta_{COI} = \frac{1}{M_T} \sum_{i=1}^{m} M_i \delta_i,\ \omega_{COI} = \frac{1}{M_T} \sum_{i=1}^{m} M_i \omega_i, \quad (3)$$

where $M_T = \sum_{i=1}^{m} M_i$.

The variables δ_i is, i-th generator interior angle, and ω_i is, i-th speed of the generator, and $\omega_s = 2\pi f$. Therefore, variables of generator in the COI frame can be rewritten as $\tilde{\delta}_i = \delta_i - \delta_{COI}$, $\tilde{\theta}_i = \theta_i - \delta_{COI}$ and $\tilde{\omega}_i = \omega_i - \omega_{COI}$. The dynamic equations of SG are as follows [30]. For the i-th generator, $i = 1, 2, \ldots, m$

$$\begin{cases} \dot{\tilde{\delta}}_i = \tilde{\omega}_i - \omega_s \\ \dot{\tilde{\omega}}_i = \dfrac{1}{M_i}\left(P_{mi} - P_{ei} - D_i\left(\tilde{\omega}_i - \omega_s\right) - \dfrac{M_i}{M_T} P_{COI}\right) \\ \dot{E}'_{qi} = \dfrac{1}{T'_{d0i}}\left(-\dfrac{x_{di}}{x'_{di}} E'_{qi} + \dfrac{x_{di} - x'_{di}}{x'_{di}} V_i cos\left(\delta_i - \theta_i\right) + E_{fi}\right) \end{cases}, \quad (4)$$

where $P_{ei} = \frac{1}{x'_{di}}\, E'_{qi} V_i \sin(\delta_i - \theta_i) - \frac{x'_{di} - x_{qi}}{2x'_{di} x_{qi}} V_i^2 \sin(2(\delta_i - \theta_i))$ and $P_{COI} = \sum_{i=1}^{m} (P_{mi} - P_{ei})$.

3.2 | DFIG modeling

The dynamic equations of DFIG have two rotor inputs, V_{dr} and V_{qr}, in the $d-q$ reference frame. With transforming to polar coordinates $E'_k = \sqrt{{E'_{dk}}^2 + {E'_{qk}}^2}$ and $\delta_k = tan^{-1}\left(\frac{E'_{qk}}{E'_{dk}}\right)$. Equivalent DFIG dynamic as follow [20]. For the k-th generator, $k = m+1, m+2 \ldots, m+l$

$$\begin{cases} \dot{\tilde{\delta}}_k = \tilde{\omega}_k - \dfrac{\left(x_{dk} - x'_{dk}\right)}{x'_{dk} T'_{0k}} \dfrac{V_k sin\left(\delta_k - \theta_k\right)}{E'_k} + \dfrac{\omega_s V_{r(k-m)} cos\left(\delta_j - \theta_{r(k-m)}\right)}{E'_k} \\ \dot{\tilde{\omega}}_k = \dfrac{1}{M_k}\left(P_{mk} - P_{ek} - \dfrac{M_k}{M_T} P_{COI}\right) \\ \dot{E}'_k = \dfrac{1}{T'_{d0k}}\left(-\dfrac{x_{dk}}{x'_{dk}} E'_k + \dfrac{x_{dk} - x'_{dk}}{x'_{dk}} V_k cos\left(\delta_k - \theta_k\right) + \omega_s T'_{d0k} V_{r(k-m)} sin\left(\delta_k - \theta_{r(k-m)}\right)\right) \end{cases}, \quad (5)$$

where θ_{rk} indicates the angle of the k-th DFIG terminal voltage V_{rk}, $V_{rk} \angle\ \theta_{rk} = V_{drk} + J\ V_{qrk} = V_{rk}\, e^{J\theta_{rk}} = |V_{rk}|\ (cos\theta_{rk} + Jsin\theta_{rk})$ and $P_{ek} = \frac{1}{x'_{dk}}\ E'_{qk} V_k \sin(\delta_k - \theta_k) - \frac{x'_{dk} - x_{qk}}{2x'_{dk} x_{qk}} V_k^2 \sin(2(\delta_k - \theta_k))$ is the active electrical power delivered via the generator to the terminal voltage V_{rk} (same as SG). $P_{COI} = \sum_{k=m+1}^{m+l} (P_{mk} - P_{ek})$.

This model of DFIG is the same as a one-axis model of an SG but has some differences [20]. The angle of the generator in the first equation of (5) includes two additional terms in comparison with the angle in the SG equation. By replacement, the 2nd and 3rd terms of the angle δ_j equation with $-S_k \omega_s$, can be written as

$$S_k = 1 + \frac{\left(x_{dk} - x'_{dk}\right)}{\omega_s x'_{dk} T'_{0k}} \frac{V_k sin\left(\delta_k - \theta_k\right)}{E'_k} - \frac{V_{r(k-m)} cos\left(\delta_k - \theta_{r(k-m)}\right)}{E'_k}, \quad (6)$$

where S_k is the rotor slip of the k-th DFIG. By blending (6) and the 3rd equation of (5) the DFIG rotor voltage inputs V_{drj} and V_{qrj} can be directly computed. Presenting the DFIG model above is beneficial because its model is the same as the SG and we can use non-linear control design methods.

4 | NOVEL NON-LINEAR CONTROL DESIGN

Lyapunov's direct method is a powerful design for transient stability analysis. This technique has been utilized to model various

controls [30, 31]. Lyapunov's theory is used to model a novel non-linear control to enhance transient stability in the power systems as follows.

Consider the dynamic models of m-SG and l-DFIG that in the form of an affine non-linear system is written as follows:

$$\begin{cases} \dot{\tilde{\delta}}_i = \widetilde{\omega}_i - \omega_s & i = 1,2,\dots,m \\ M_i\dot{\widetilde{\omega}}_i = P_{mi} - P_{ei} - D_i(\widetilde{\omega}_i - \omega_s) - \dfrac{M_i}{M_T}P_{COI} \\ \dfrac{T'_{d0i}}{x_{di}-x'_{di}}\dot{E}'_i = -\dfrac{x_{di}}{x'_{di}(x_{di}-x'_{di})}E'_i + \dfrac{V_i cos(\delta_i-\theta_i)}{x'_{di}} + \dfrac{1}{(x_{di}-x'_{di})}E_{fi} \\ \dot{\tilde{\delta}}_k = \widetilde{\omega}_k - S_k\omega_s & k = m+1,\dots,m+l \\ M_k\dot{\widetilde{\omega}}_k = P_{mk} - P_{ek} - \dfrac{M_k}{M_T}P_{COI} \\ \dfrac{T'_{d0k}}{x_{dk}-x'_{dk}}\dot{E}'_k = -\dfrac{x_{dk}}{x'_{dk}(x_{dk}-x'_{dk})}E'_k + \dfrac{V_k cos(\delta_k-\theta_k)}{x'_{dk}} + \dfrac{1}{(x_{dk}-x'_{dk})}\omega_s T'_{d0k}V_{r(k-m)}sin(\delta_k-\theta_{r(k-m)}) \end{cases} \tag{7}$$

A TEF that includes SG and DFIG can be expressed as below:

$$\begin{aligned} v_{(\tilde{\delta},\tilde{\omega},E',V,\tilde{\theta})} &= v_k + \sum_{i=1}^{8} v_{pi} + v_0 \\ v_k &= \frac{1}{2}\sum_{i=1}^{m} M_i(\widetilde{\omega}_i-\omega_s)^2 + \frac{1}{2}\sum_{k=m+1}^{m+l} M_k\left(\widetilde{\omega}_k - S_{k(\tilde{\delta},E',V,\tilde{\theta})}\omega_s\right)^2 \\ v_{p1} &= -\sum_{i=1}^{m+l} P_{mi}\tilde{\delta}_i \\ v_{p2} &= \sum_{i=m+l+1}^{m+l+n} P_{Li}\tilde{\theta}_i \\ v_{p3} &= \sum_{i=m+l+1}^{m+l+n} \int \frac{Q_{Li}}{V_i}dV_i \\ v_{p4} &= \sum_{i=1}^{m+l}\frac{1}{2x'_{di}}\left[E_i'^2 + V_i^2 - 2E'_iV_i\cos(\delta_i-\theta_i)\right] \\ v_{p5} &= -\frac{1}{2}\sum_{i=1}^{m+l+n}\sum_{j=1}^{m+k+n} B_{ij}V_iV_j\cos(\theta_i-\theta_j) \\ v_{p6} &= \sum_{i=1}^{m+l}\frac{x'_{di}-x_{qi}}{4x'_{di}x_{qi}}\left[V_i^2 - V_i^2\cos(2(\delta_i-\theta_i))\right] \\ v_{p7} &= -\sum_{i=1}^{m}\frac{E'_i}{x_{di}-x'_{di}}E_{fi} - \sum_{k=m+1}^{m+l}\frac{E'_k}{x_{dk}-x'_{dk}}\omega_s T'_{d0k}V_{r(k-m)} cos(\delta_k-\theta_{r(k-m)}) \\ v_{p8} &= \sum_{i=1}^{m+l}\frac{E_i'^2}{2(x_{di}-x'_{di})} \end{aligned} \tag{8}$$

By utilizing the symbol $[\frac{dv}{dt}]_{\tilde{\omega}}$ for $\frac{\partial v}{\partial\tilde{\omega}}\frac{d\tilde{\omega}}{dt}$ and $\dot{S}_{(\tilde{\delta})}$ for $\frac{\partial S}{\partial\tilde{\delta}}$ the same way for the other cases, we have:

$$\begin{aligned} &\left[\frac{dv_K}{dt}\right]_{\tilde{\omega}} + \left[\frac{dv_k}{dt}+\frac{dv_{p1}}{dt}+\frac{dv_{p4}}{dt}+\frac{dv_{p6}}{dt}+\frac{dv_{p7}}{dt}\right]_{\tilde{\delta}} = \\ &-\sum_{i=1}^{m} D_i(\widetilde{\omega}_i-\omega_s)^2 - \sum_{k=m+1}^{m+l} M_k\omega_s(\widetilde{\omega}_k - S_k\omega_s)^2\dot{S}_{k(\tilde{\delta})} \\ &+\sum_{k=m+1}^{m+l}\frac{E'_k}{x_{dk}-x'_{dk}}\omega_s T'_{d0k}V_{r(k-m)}sin(\delta_k-\theta_{r(k-m)})(\widetilde{\omega}_k - S_k\omega_s) \end{aligned} \tag{9.a}$$

$$\left[\frac{dv_K}{dt}+\frac{dv_{p2}}{dt}+\frac{dv_{p4}}{dt}+\frac{dv_{p5}}{dt}+\frac{dv_{p6}}{dt}\right]_{\tilde{\theta}} = \sum(P_i+P_{Li})\dot{\tilde{\theta}}_i - \sum_{k=m+1}^{m+l} M_k\omega_s(\widetilde{\omega}_k - S_k\omega_s)\dot{S}_{k(\tilde{\theta})}\dot{\tilde{\theta}}_k, \tag{9.b}$$

$$\left[\frac{dv_K}{dt}+\frac{dv_{p3}}{dt}+\frac{dv_{p4}}{dt}+\frac{dv_{p5}}{dt}+\frac{dv_{p6}}{dt}\right]_{V} = \sum(Q_i+Q_{Li})\frac{\dot{V}_i}{V_i} - \sum_{k=m+1}^{m+l} M_k\omega_s(\widetilde{\omega}_k - S_k\omega_s)\dot{S}_{k(V)}\dot{V}_k, \tag{9.c}$$

$$\left[\frac{dv_K}{dt}+\frac{dv_{p7}}{dt}+\frac{dv_{p8}}{dt}+\frac{dv_{p4}}{dt}\right]_{E'_q} = -\sum_{i=1}^{m}\frac{T'_{d0i}}{x_{di}-x'_{di}}\dot{E}_i'^2 - \sum_{k=m+1}^{m+l} M_k\omega_s(\widetilde{\omega}_k - S_k\omega_s)\dot{S}_{k(E'_k)}\dot{E}'_k, \tag{9.d}$$

where $\sum(P_i+P_{Li})\dot{\tilde{\theta}}_i = 0$ and $\sum(Q_i+Q_{Li})\frac{\dot{V}_i}{V_i} = 0$

4.1 | Design of DFIG controller

The time-derivative of the TEF that includes SG and DFIG is as follows:

$$\begin{aligned} \dot{v} = &-\left[\sum_{i=1}^{m} D_i(\widetilde{\omega}_i-\omega_s)^2 + \sum_{i=1}^{m}\frac{T'_{d0i}}{x_{di}-x'_{di}}\dot{E}_i'^2\right] \\ &-\left[\begin{array}{l} \sum_{k=m+1}^{m+l} M_k\omega_s(\widetilde{\omega}_k - S_k\omega_s)^2\dot{S}_{k(\tilde{\delta})} \\ \quad -\sum_{k=m+1}^{m+l}\frac{E'_k}{x_{dk}-x'_{dk}}\omega_s T'_{d0k}V_{r(k-m)}sin(\delta_k-\theta_{r(k-m)}) \\ (\widetilde{\omega}_k - S_k\omega_s) + \sum_{k=m+1}^{m+l} M_k\omega_s(\widetilde{\omega}_k - S_k\omega_s)\dot{S}_{k(\tilde{\theta})}\dot{\tilde{\theta}}_k \\ \quad + \sum_{k=m+1}^{m+l} M_k\omega_s(\widetilde{\omega}_k - S_k\omega_s)\dot{S}_{k(V)}\dot{V}_k \\ \quad + \sum_{k=m+1}^{m+l} M_k\omega_s(\widetilde{\omega}_k - S_k\omega_s)\dot{S}_{k(E'_k)}\dot{E}'_k \end{array}\right], \\ = &\dot{v}_{SG} + \dot{v}_{DFIG} \end{aligned} \tag{10}$$

where $\dot{S}_{k(\delta)}$, $\dot{S}_{k(E')}$, $\dot{S}_{k(V)}$ and $\dot{S}_{k(\tilde{\theta})}$ are given in Appendix A.

$$\dot{v}_{DFIG} = -\sum_{k=m+1}^{m+l} M_k\omega_s\left(\widetilde{\omega_k} - S_k\omega_s\right)\left(-\frac{E'_k T'_{d0k}}{M_k\left(x_{dk}-x'_{dk}\right)}V_{r(k-m)}\right.$$
$$\left. sin\left(\delta_k - \theta_{r(k-m)}\right) + \dot{S}_{k(\delta)}\dot{\tilde{\delta}}_k + \dot{S}_{k(\tilde{\theta})}\dot{\tilde{\theta}}_k + \dot{S}_{k(V)}\dot{V}_k + \dot{S}_{k(E')}\dot{E}'_k\right). \tag{11.a}$$

By using $V_r sin\ (\delta - \theta_r) = V_{dr}\ \ sin\delta - V_{qr} cos\delta$ and $V_r sin\ (\delta - \theta_r) = V_r\ (cos\theta_r sin\delta - sin\theta_r cos\delta)$, we have:

$$\dot{v}_{DFIG} = -\sum_{k=m+1}^{m+l}\left(\begin{array}{l}\left[M_k\omega_s\left(\widetilde{\omega_k} - S_k\omega_s\right)\left(-V_{drk}\frac{E'_k T'_{d0k} sin\delta_k}{M}{}_k\left(x_{dk}-x'_{dk}\right)\right)\right.\\ \left.+\ \dot{S}_{k(\tilde{\delta})}\left(\widetilde{\omega_k} - S_k\omega_s\right) + \dot{S}_{k(\tilde{\theta})}\dot{\tilde{\theta}}_k + \dot{S}_{k(V)}\dot{V}_k + \dot{S}_{k(E')}\dot{E}'_k\right)\Big]\\ +\left[M_k\omega_s\left(\widetilde{\omega_k} - S_k\omega_s\right)\left(V_{qrk}\frac{E'_k T'_{d0k} cos\delta_k}{M}{}_{k(x_{dk}-x'_{dk})}\right)\right]\end{array}\right). \tag{11.b}$$

If $\dot{v}_{DFIG}$ is negative. The DFIG aids to the system oscillation damping. To achieve this aim:

$$U_{drk} = -K_r\frac{M_k\left(x_{dk}-x'_{dk}\right)}{E'_k T'_{d0k}} sin\left(\delta_k\right)\left[\left(\widetilde{\omega_k} - S_k\omega_s\right)\left(1-\dot{S}_{k(\delta)}\right)\right.$$
$$\left. -\ \dot{S}_{k(\tilde{\theta})}\dot{\tilde{\theta}}_k - \dot{S}_{k(V)}\dot{V}_k - \dot{S}_{k(E')}\dot{E}'_k\right], \tag{12.a}$$

$$U_{qrk} = K_r\ \frac{M_k\left(x_{dk}-x'_{dk}\right)}{E'_k T'_{d0k}} cos\left(\delta_k\right)\left(\widetilde{\omega_k} - S_k\omega_s\right), \tag{12.b}$$

where K_{rd} and K_{rq} are positive constants that are chosen separately to acquire proper damping of fluctuations. By selecting U_{drk} and U_{qrk} as given by (12), (10) becomes:

$$\dot{v} = -\sum_{i=1}^{m} D_i(\widetilde{\omega_i} - \omega_s)^2 - \sum_{i=1}^{m}\frac{T'_{d0i}}{x_{di}-x'_{di}}\dot{E}'^2_{qi}$$
$$-\sum_{k=m+1}^{m+l} K_r M_k\omega_s\left(\widetilde{\omega_k} - S_k\omega_s\right)^2 \le 0. \tag{13}$$

4.2 | Design of UPFC controller

The offering of the UPFC does not modify the TEF (8) but does alter $\dot{v}$. When the UPFC is placed between buses i and j, we have:

$$\left[\frac{dv_k}{dt} + \frac{dv_{p2}}{dt} + \frac{dv_{p4}}{dt} + \frac{dv_{p5}}{dt} + \frac{dv_{p6}}{dt}\right]_{\tilde{\theta}} = -P_{ui}\dot{\tilde{\theta}}_i - P_{uj}\dot{\tilde{\theta}}_j$$
$$-\sum_{j=m+1}^{m+l} M_j\omega_s\left(\widetilde{\omega_j} - S_j\omega_s\right)\dot{S}_{j(\tilde{\theta})}\dot{\tilde{\theta}}_j, \tag{14.a}$$

$$\left[\frac{dv_k}{dt} + \frac{dv_{p3}}{dt} + \frac{dv_{p4}}{dt} + \frac{dv_{p5}}{dt} + \frac{dv_{p6}}{dt}\right]_V = -Q_{ui}\frac{\dot{V}_i}{V_i} - Q_{uj}\frac{\dot{V}_j}{V_j}$$
$$-\sum_{j=m+1}^{m+l} M_j\omega_s\left(\widetilde{\omega_j} - S_j\omega_s\right)\dot{S}_{j(V)}\dot{V}_j. \tag{14.b}$$

Since for the UPFC $P_{ui} = -P_{uj}$, so $\dot{v}$ is written as follows:

$$\dot{v} = -\left[\begin{array}{l}\sum_{i=1}^{m} D_i(\widetilde{\omega_i} - \omega_s)^2 + \sum_{i=1}^{m}\frac{T'_{d0i}}{x_{di}-x'_{di}}\dot{E}_i'^2 + \sum_{k=m+1}^{m+l} M_k\omega_s\left(\widetilde{\omega_k} - S_k\omega_s\right)^2\dot{S}_{k(\delta)}\\ -\sum_{k=m+1}^{m+l}\frac{E'_k}{x_{dk}-x'_{dk}}\omega_s T'_{d0k}V_{r(k-m)}sin\left(\delta_k - \theta_{r(k-m)}\right)\left(\widetilde{\omega_k} - S_k\omega_s\right)\\ +\sum_{k=m+1}^{m+l} M_k\omega_s\left(\widetilde{\omega_k} - S_k\omega_s\right)\dot{S}_{k(\tilde{\theta})}\dot{\tilde{\theta}}_k\\ +\sum_{k=m+1}^{m+l} M_k\omega_s\left(\widetilde{\omega_k} - S_k\omega_s\right)\dot{S}_{k(V)}\dot{V}_k + \sum_{k=m+1}^{m+l} M_k\omega_s\left(\widetilde{\omega_k} - S_k\omega_s\right)\dot{S}_{k(E'_k)}\dot{E}'_k\end{array}\right],$$
$$-\left[P_{ui}\dot{\widetilde{\theta}}_{ij} + Q_{ui}\frac{\dot{V}_i}{V_i} + Q_{uj}\frac{\dot{V}_j}{V_j}\right] = \dot{v}_{no_{upfc}} + \dot{v}_{upfc} \tag{15}$$

where $\dot{v}_{upfc} = -[P_{ui}\dot{\widetilde{\theta}}_{ij} + Q_{ui}\frac{\dot{V}_i}{V_i} + Q_{uj}\frac{\dot{V}_j}{V_j}]$. By substituting the power flow of UPFC (2), we have

$$\dot{v}_{upfc} = -B_{se}\left[V_{sed}\left(\dot{V}_i - \dot{V}_j cos\theta_{ij}\right) + V_{seq}\left(V_i\omega_{ij} + \dot{V}_j sin\theta_{ij}\right)\right]$$
$$-B_{sh}\left[V_i V_{shq}\omega_{ij} + V_{shd}\dot{V}_i\right], \tag{16}$$

where $\theta_{ij} = \theta_i - \theta_j$, $\dot{\tilde{\theta}}_{ij} = \dot{\tilde{\theta}}_i - \dot{\tilde{\theta}}_j$, $\omega_{ij} = \dot{\tilde{\theta}}_{ij} = \dot{\theta}_{ij}$.

If $\dot{v}_{upfc}$ is negative, the UPFC aids to dampen the oscillation of the system. To achieve this aim:

$$U_{sed} = k_{sd}\ \left(\dot{V}_i - \dot{V}_j cos\theta_{ij}\right), \tag{17.a}$$

$$U_{seq} = k_{sq}\ \left(V_i\omega_{ij} + \dot{V}_j sin\theta_{ij}\right), \tag{17.b}$$

$$U_{shd} = k_{hd}\ \dot{V}_i, \tag{17.c}$$

$$U_{shq} = k_{hq}\ V_i\omega_{ij}, \tag{17.d}$$

where k_{sd}, k_{sq}, k_{hd} and k_{hq} are positive constants that are chosen separately to acquire proper damping of fluctuations. By selecting U_{dri} and U_{qri} as given by (12) and V_{sed}, V_{seq}, V_{shd} and V_{shq} as given by (17), (15) becomes:

$$\dot{v} = -\left[\sum_{i=1}^{m} D_i(\widetilde{\omega_i} - \omega_s)^2 + \sum_{i=1}^{m}\frac{T'_{d0i}}{x_{di}-x'_{di}}\dot{E}'^2_{qi}\right]$$
$$-\left[\sum_{k=m+1}^{m+l} k_r M_k\omega_s\left(\widetilde{\omega_k} - S_k\omega_s\right)^2\right]$$

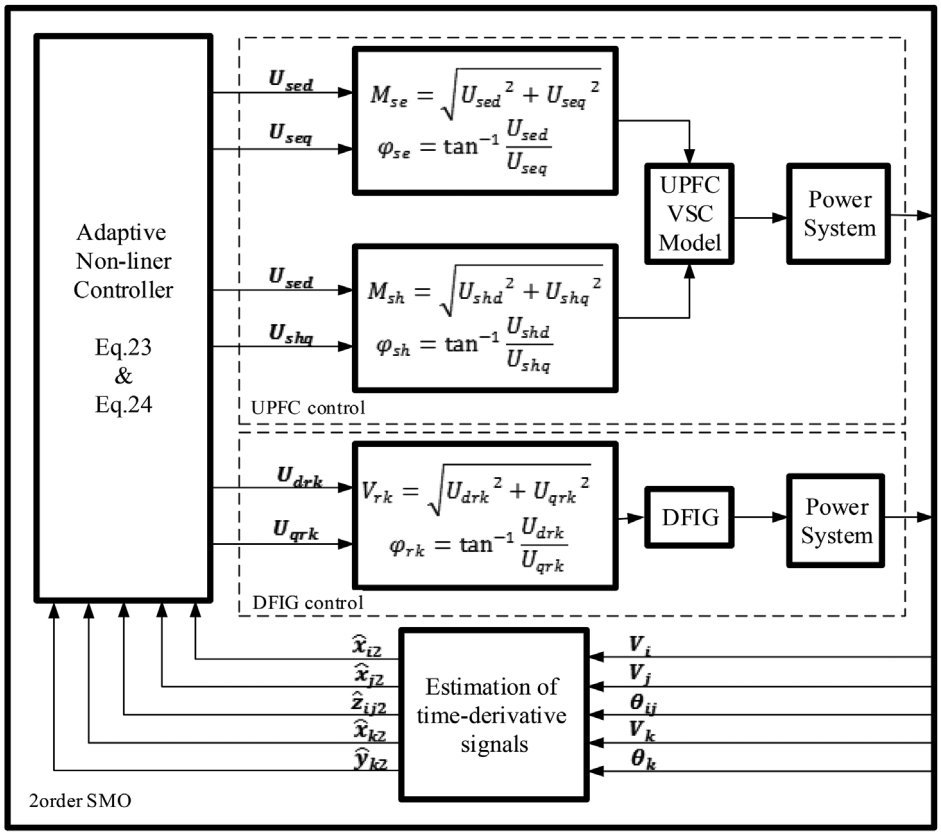

FIGURE 2 The novel non-linear control configuration

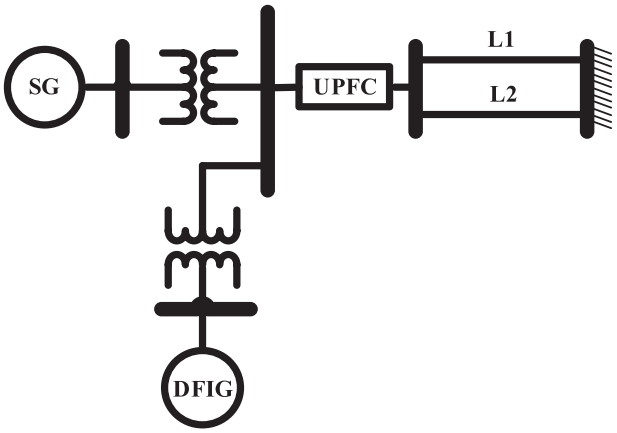

FIGURE 3 The TMIB system

$$-\left[B_{se}K_{sd}\left(\dot{V}_i - \dot{V}_j cos\theta_{ij}\right)^2 + B_{se}K_{sq}\left(V_i\omega_{ij} + \dot{V}_j sin\theta_{ij}\right)^2 + B_{sh}K_{hq}\left(V_i\omega_{ij}\right)^2 + B_{sh}K_{hd}\left(\dot{V}_i\right)^2\right] = \dot{v}_{SG} + \dot{v}_{DFIG} + \dot{v}_{upfc} \le 0. \quad (18)$$

Thus, damping of oscillation in the power system is happening by providing the DFIG and UPFC controlled with (12) and (17).

The control laws include time-derivatives. The $\dot{V}_i$, $\dot{V}_j$, $\dot{V}_k$, $\dot{\theta}_k$ and $\dot{\theta}_{ij}$ due to the presence of noise, cannot be obtained directly by numerical differentiation. To deal with this problem, a second sliding mode observer is used to estimate control parameters in Section 4.3.

4.3 | States observer design

To estimate the unavailable voltage and angle derivatives required for the implementation of the novel controller, let's consider second-order sliding mode observer and then we introduce the variables as follows:

$$\begin{aligned} x_{s1} &= V_s \\ \dot{x}_{s1} &= x_{s2} = \dot{V}_s, s = i, j, k \end{aligned}, \quad (19.a)$$

$$\begin{aligned} y_{k1} &= \theta_k \\ \dot{y}_{k1} &= y_{k2} = \dot{\theta}_k \end{aligned}, \quad (19.b)$$

$$\begin{aligned} z_{ij1} &= \theta_{ij} \\ \dot{z}_{ij1} &= z_{ij2} = \dot{\theta}_{ij} \end{aligned}. \quad (19.c)$$

Assuming the measurable voltages and angles (V_s, $s = i, j, k$;θ_k ;θ_{ij}) are continuous and bounded, improved

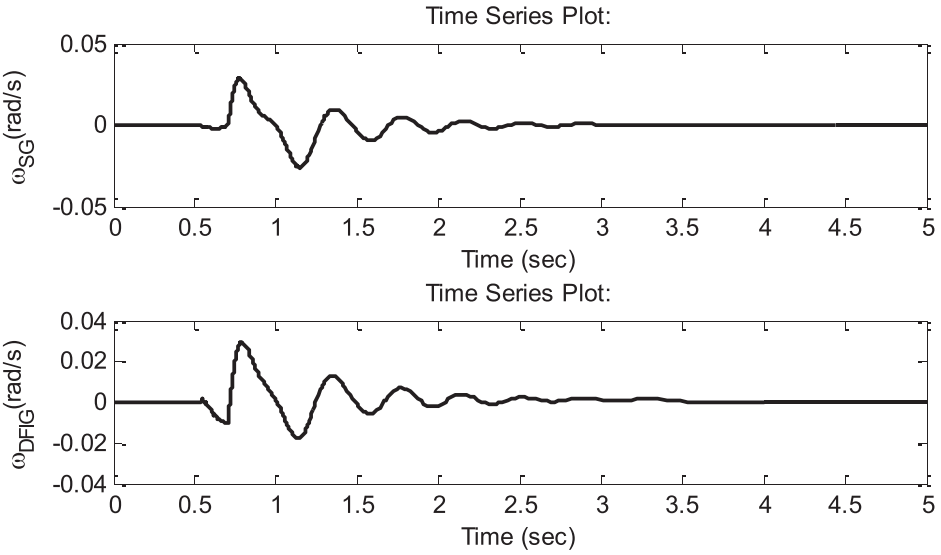

FIGURE 4 The speed of SG and DFIG

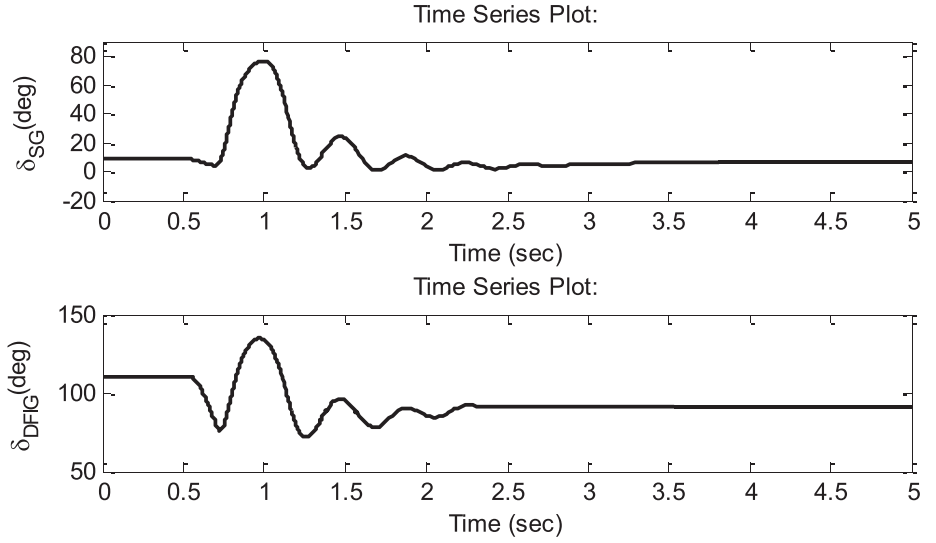

FIGURE 5 The rotor angle of SG and DFIG

TABLE 1 CCT for different controls in TMIB

System with	Controller	CCT (ms)
UPFC	Without	214
	Novel	252
DFIG		257
UPFC & DFIG		264

second-order sliding mode observers are written as follows [34, 35]:

$$\begin{aligned}\dot{\hat{x}}_{s1} &= \hat{x}_{s2} + w_{1x},\ s = i,\ j,\ k\\ \dot{\hat{x}}_{s2} &= w_{2x}\end{aligned}, \tag{20.a}$$

$$\begin{aligned}\dot{\hat{y}}_{k1} &= \hat{y}_{k2} + w_{1y}\\ \dot{\hat{y}}_{k2} &= w_{2y}\end{aligned}, \tag{20.b}$$

$$\begin{aligned}\dot{\hat{z}}_{ij1} &= \hat{z}_{ij2} + w_{1z}\\ \dot{\hat{z}}_{ij2} &= w_{2z}\end{aligned}, \tag{20.c}$$

where the variables w_{1x}, w_{2x}, w_{1y}, w_{2y}, w_{1z}, and w_{2z} are given by the following expressions:

$$\begin{aligned}w_{1x} &= -\beta_x|\hat{x}_{s1} - x_{s1}|^{\frac{1}{2}} sign\,(\hat{x}_{s1} - x_{s1}) - K_x\,(\hat{x}_{s1} - x_{s1})\\ w_{2x} &= -\alpha_x sign\,(\hat{x}_{s1} - x_{s1})\end{aligned}, \tag{21.a}$$

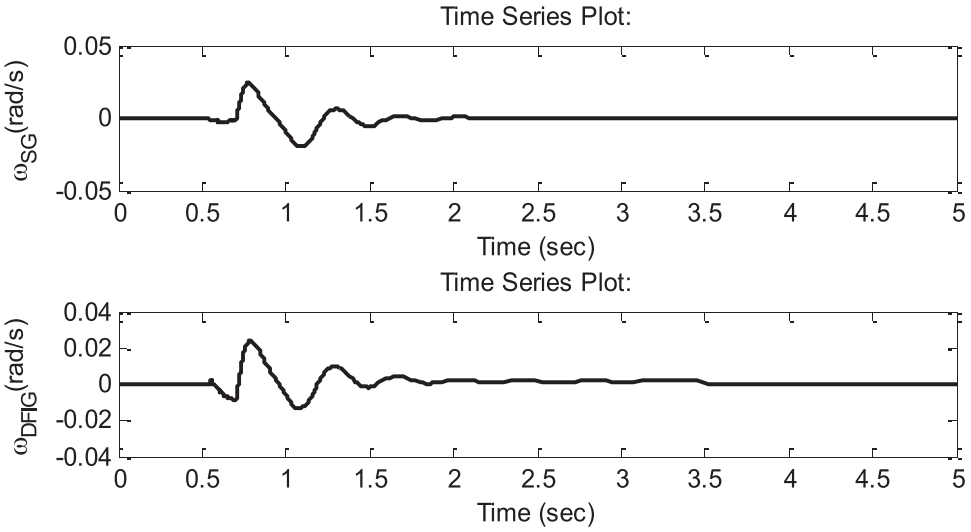

FIGURE 6 The speed of SG and DFIG in which L1 is removed

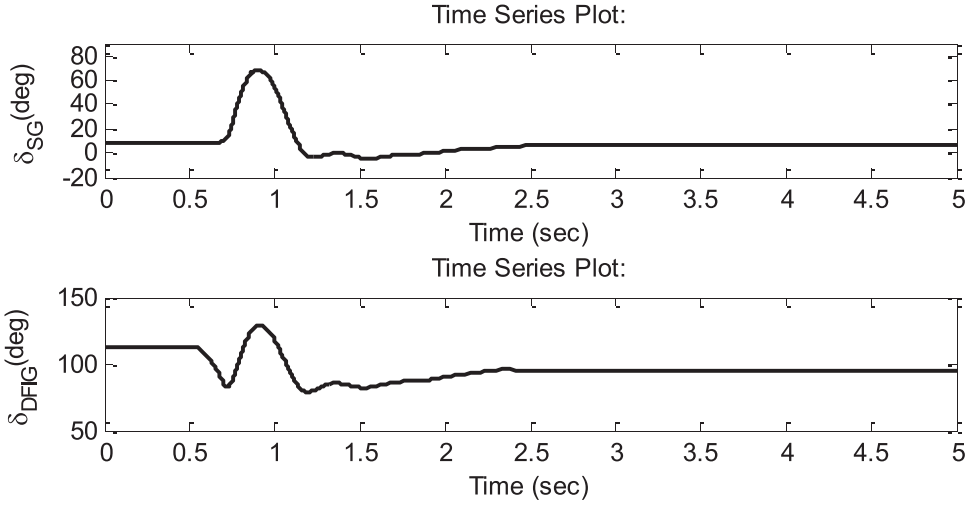

FIGURE 7 The rotor angle of SG and DFIG in which L1 is removed

TABLE 2 CCT for different controls and faults in IEEE 9-bus test system

	CCT (ms) for different controls			
Fault line	**Without**	**POD**	**Backstepping**	**Novel**
4-5	134	161	165	176
4-6	141	168	172	181

$$w_{1y} = -\beta_y\left|\hat{y}_{k1} - y_{k1}\right|^{\frac{1}{2}} sign\left(\hat{y}_{k1} - y_{k1}\right) - K_y\left(\hat{y}_{k1} - y_{k1}\right),$$
$$w_{2y} = -\alpha_y sign\left(\hat{y}_{k1} - y_{k1}\right) \tag{21.b}$$

$$w_{1\tilde{z}} = -\beta_{\tilde{z}}\left|\hat{\tilde{z}}_{ij1} - \tilde{z}_{ij1}\right|^{\frac{1}{2}} sign\left(\hat{\tilde{z}}_{ij1} - \tilde{z}_{ij1}\right) - K_{\tilde{z}}\left(\hat{\tilde{z}}_{ij1} - \tilde{z}_{ij1}\right),$$
$$w_{2\tilde{z}} = -\alpha_{\tilde{z}} sign\left(\hat{\tilde{z}}_{ij1} - \tilde{z}_{ij1}\right) \tag{21.c}$$

α_r, β_r, and K_r ($r = x, y, \tilde{z}$) are the positive tuning parameters. Taking $e_{x_{s1}} = \hat{x}_{s1} - x_{s1}$, $e_{x_{s2}} = \hat{x}_{s2} - x_{s2}$, $e_{y_{k1}} = \hat{y}_{k1} - y_{k1}$, $e_{y_{k2}} = \hat{y}_{k2} - y_{k2}$, $e_{\tilde{z}_{ij1}} = \hat{\tilde{z}}_{ij1} - \tilde{z}_{ij1}$, and $e_{\tilde{z}_{ij2}} = \hat{\tilde{z}}_{ij2} - \tilde{z}_{ij2}$ the following dynamics errors equations are acquired:

$$\dot{e}_{x_{s1}} = -K_x e_{x_{s1}} - \beta_x\left|e_{x_{s1}}\right|^{\frac{1}{2}} sign\left(e_{x_{s1}}\right),$$
$$\dot{e}_{x_{s2}} = -\alpha_x sign\left(e_{x_{s1}}\right) \tag{22.a}$$

$$\dot{e}_{y_{k1}} = -K_y e_{y_{k1}} - \beta_y\left|e_{y_{k1}}\right|^{\frac{1}{2}} sign\left(e_{y_{k1}}\right),$$
$$\dot{e}_{y_{k2}} = -\alpha_y sign\left(e_{y_{k1}}\right) \tag{22.b}$$

$$\dot{e}_{\tilde{z}_{ij1}} = -K_{\tilde{z}} e_{\tilde{z}_{ij1}} - \beta_y\left|e_{\tilde{z}_{ij1}}\right|^{\frac{1}{2}} sign\left(e_{\tilde{z}_{ij1}}\right).$$
$$\dot{e}_{\tilde{z}_{ij2}} = -\alpha_{\tilde{z}} sign\left(e_{\tilde{z}_{ij1}}\right) \tag{22.c}$$

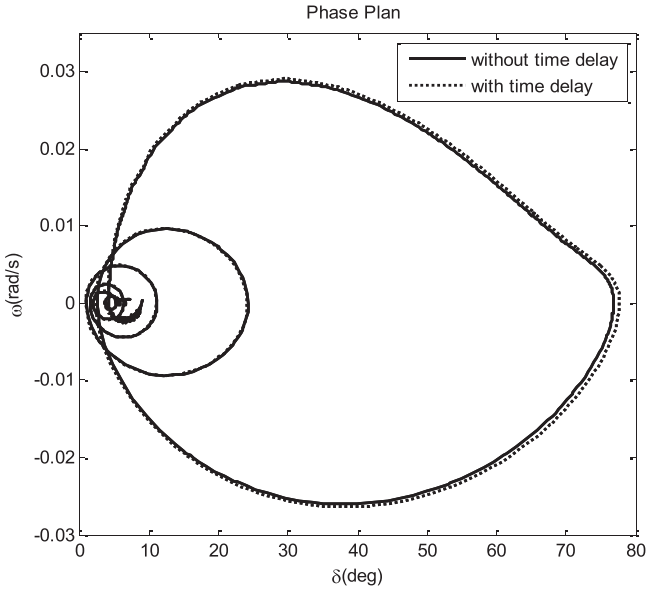

FIGURE 8 Impact of variable time delay in control signals

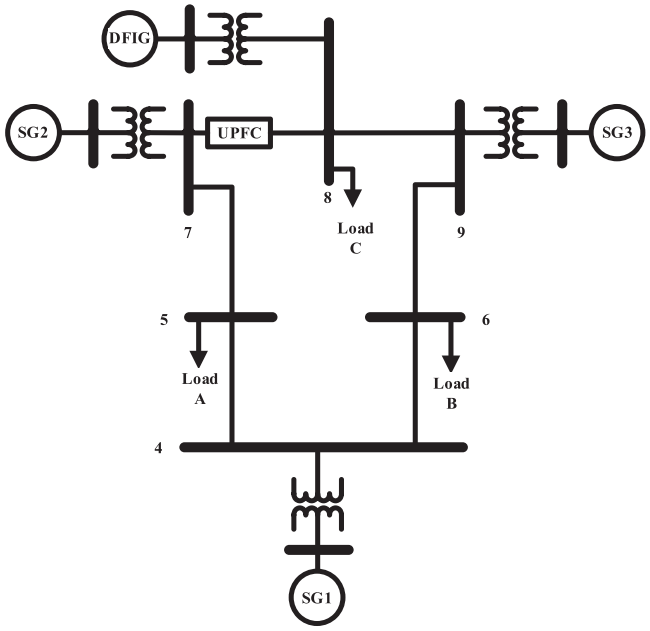

FIGURE 9 The IEEE 9-bus system with DFIG and UPFC

It is demonstrated in Sections 4.1 and 4.2 that the introduction of the DFIG and UPFC by a non-adaptive controller provides additional damping of oscillation. Thus, the estimated parameters are substituted in the controller and finally, the adaptive controller for the k-th DFIG and UPFC is as follows:

$$U_{drk} = -K_r \frac{M_k\left(x_{dk}-x'_{dk}\right)}{E'_k T'_{d0k}} sin\left(\delta_k\right)\left[\left(\omega_k - S_k\omega_s\right)\left(1-\dot{S}_{k(\tilde{\delta})}\right)\right.$$
$$\left. - \dot{S}_{k(\tilde{\theta})}\hat{y}_{k2} - \dot{S}_{k(V)}\hat{x}_{k2} - \dot{S}_{k(E')}\dot{E}'_k\right] \quad (23.a)$$

$$U_{qrk} = K_r \frac{M_k\left(x_{dk}-x'_{dk}\right)}{E'_k T'_{d0k}} cos\left(\delta_k\right)\left(\omega_k - S_k\omega_s\right) \quad (23.b)$$

$$U_{sed} = K_{sd}\left(\hat{x}_{i2} - \hat{x}_{j2}cos\theta_{ij}\right) \quad (24.a)$$

$$U_{seq} = K_{sq}\left(V_i\hat{z}_{ij2} + \hat{x}_{j2}sin\theta_{ij}\right) \quad (24.b)$$

$$U_{shq} = K_{hq}\, V_i\hat{z}_{ij2} \quad (24.c)$$

$$U_{shd} = K_{hd}\,\hat{x}_{i2} \quad (24.d)$$

Figure 2 indicates the layout of the novel non-linear control, which consists of three parts. Its two parts are related to the primary control schemed by TEF for UPFC and DFIG, and the third part is related to supplementary damping control expanded by the second-order sliding mode. The input voltages and angles in the second-order sliding mode controller (V_i, V_j, V_k, θ_k, θ_{ij}) via the DFIG and UPFC terminal bus are measured.

5 | SIMULATION DESIGN

The performance of the novel non-linear control is done with numerical simulations in MATLAB software. Although the formulations were obtained using the one-axis model of SG and DFIG, the simulations were performed with their complete model in the Simulink MATLAB environment.

5.1 | TMIB

The TMIB system, shown in Figure 3, includes SG, DFIG, and UPFC providing the system power which is transferred via two transmission lines. In the TMIB system, the infinite bus provides the voltage source by constant magnitude and angle. The parameters of the TMIB system and UPFC are given in appendix B and C, respectively.

A three-phase fault, the worst fault of real power systems, happens at the end of line L1. The value of Critical Clearing Time (CCT) for the uncompensated TMIB system is equal to 0.214. For the compensated system with UPFC and DFIG, CCT recalculation is performed. Table 1 presents CCT results for the different systems and controllers.

The large three-phase disturbances considered in this design are equal to 0.2 s which is happens at 0.5 s and is removed at 0.7 s. According to Figures 4 and 5, the novel control method helps to increase transient stability and damping of oscillation, especially in the first swing. In Figures 6 and 7, the disturbance clearance is performed via removing the line L1, which demonstrates the robustness of the new control method versus system topology changes.

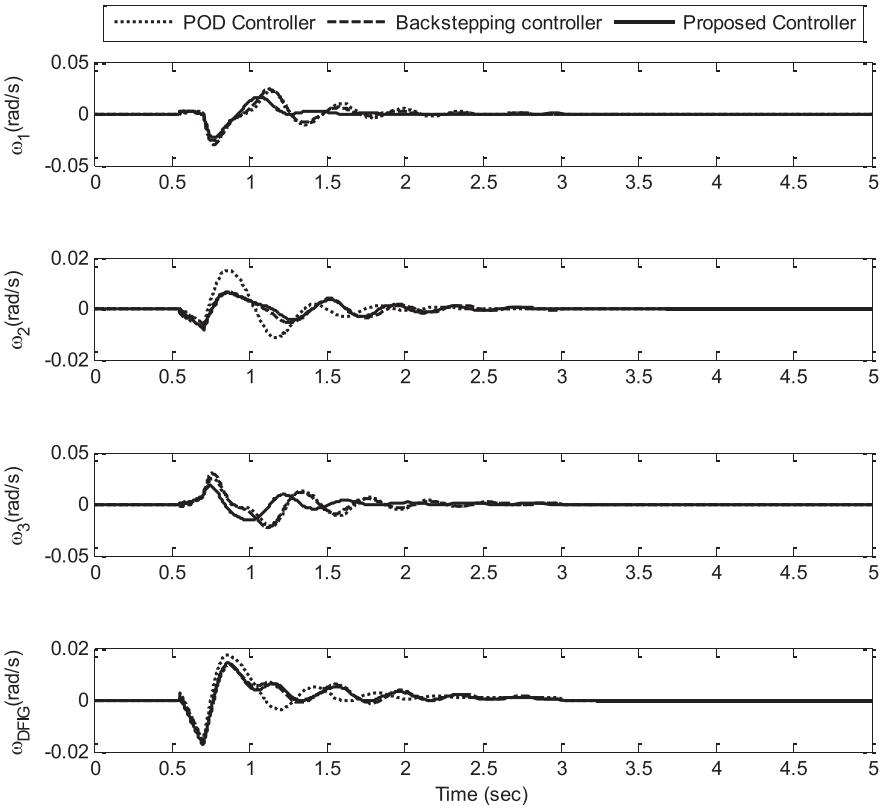

FIGURE 10 The speed of SGs 1, 2, 3, and DFIG

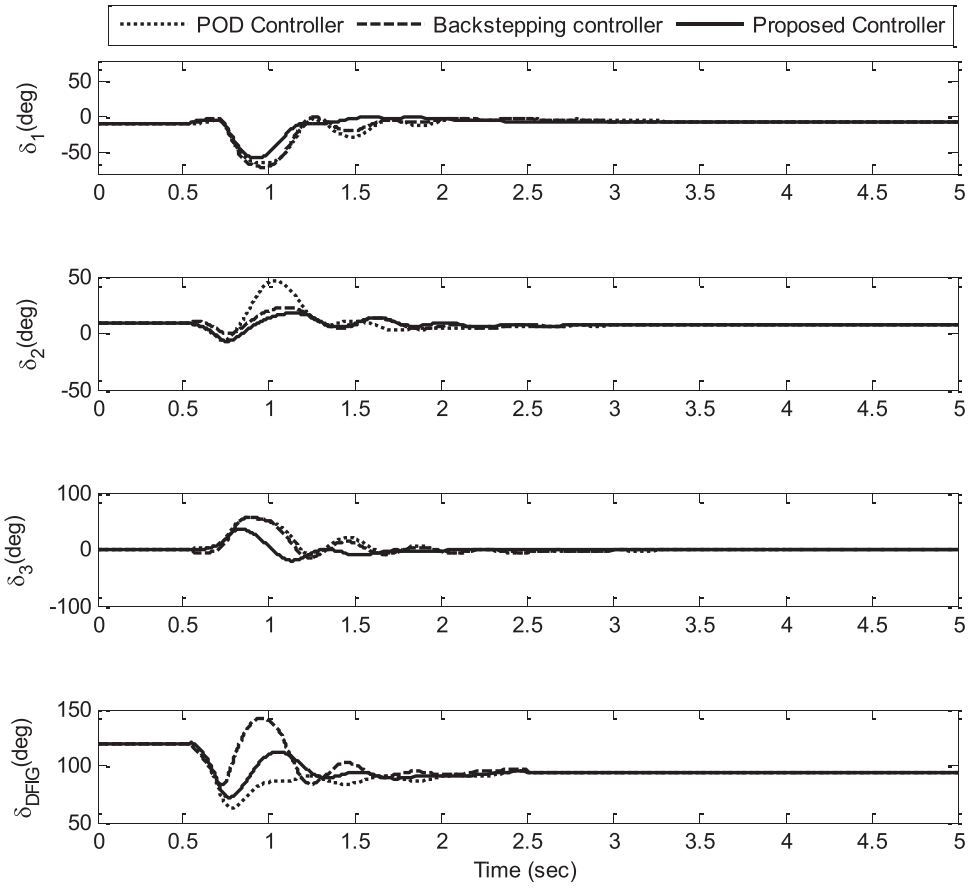

FIGURE 11 The rotor angle of SGs 1, 2, 3, and DFIG

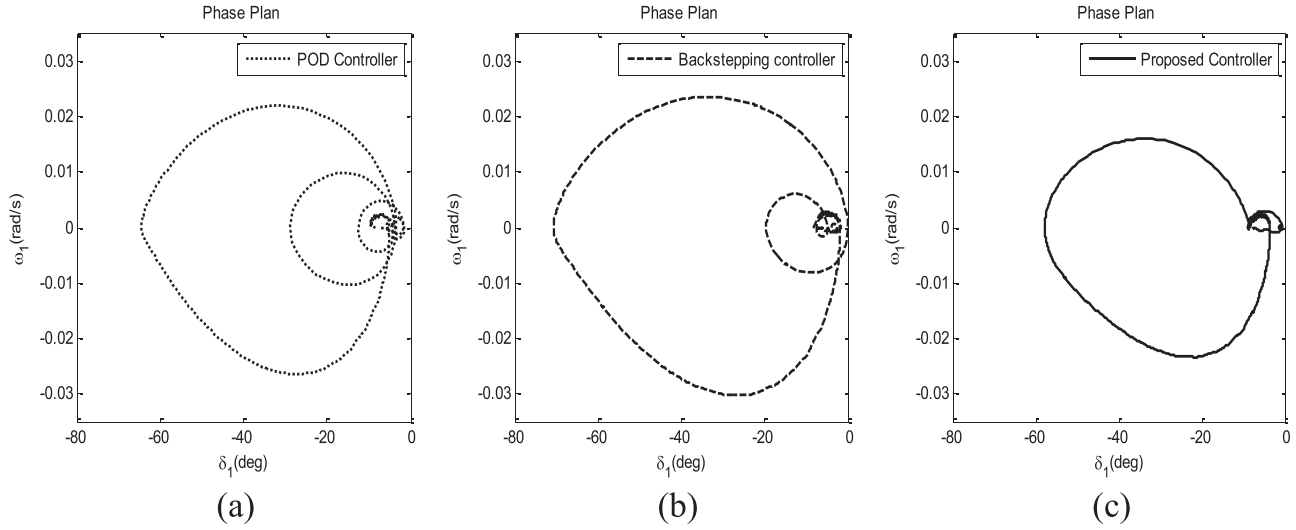

FIGURE 12 Phase plan: (a) The POD controller; (b) the backstepping controller; (c) the proposed non-linear controller

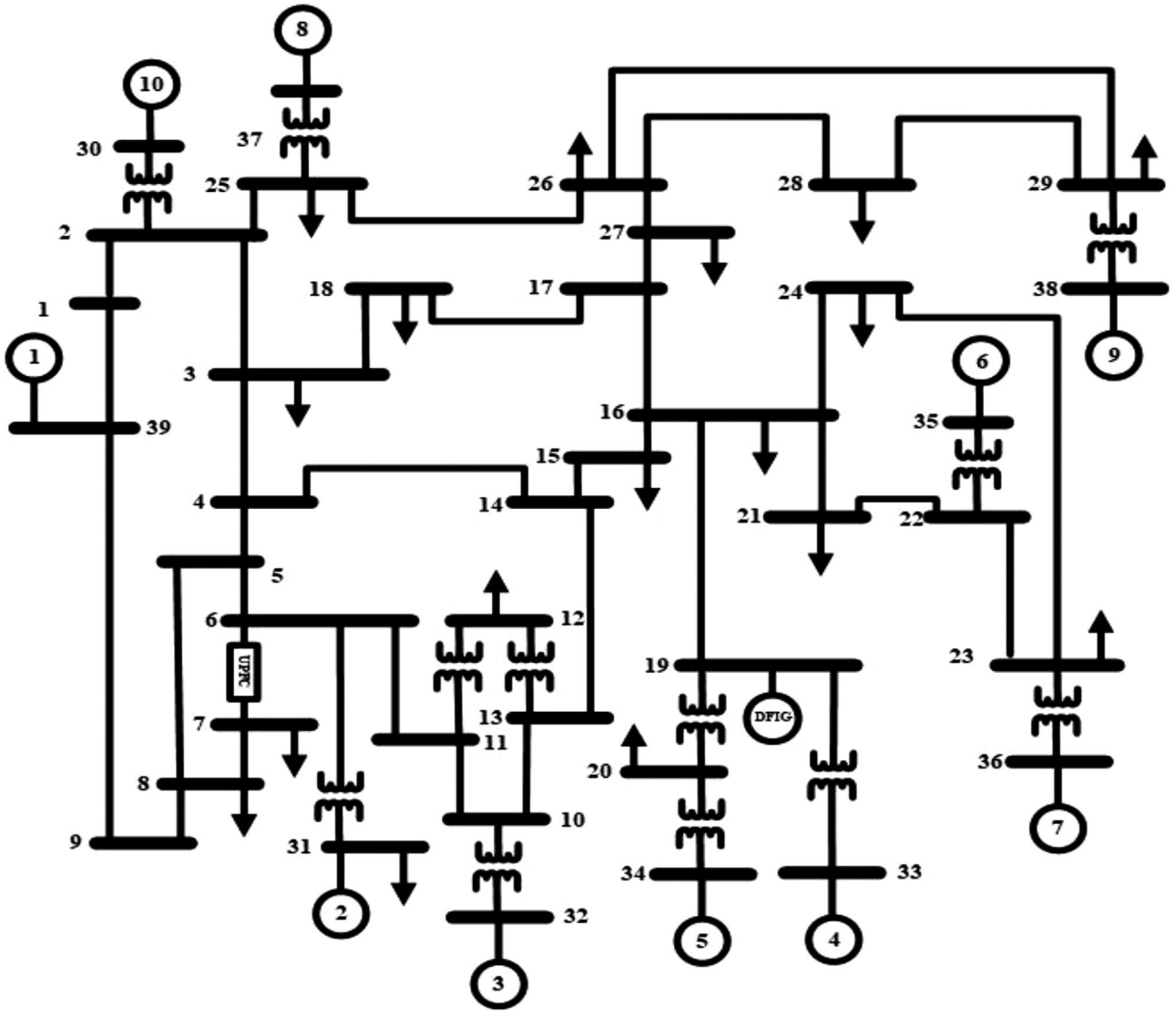

FIGURE 13 The New England power system network single line diagram

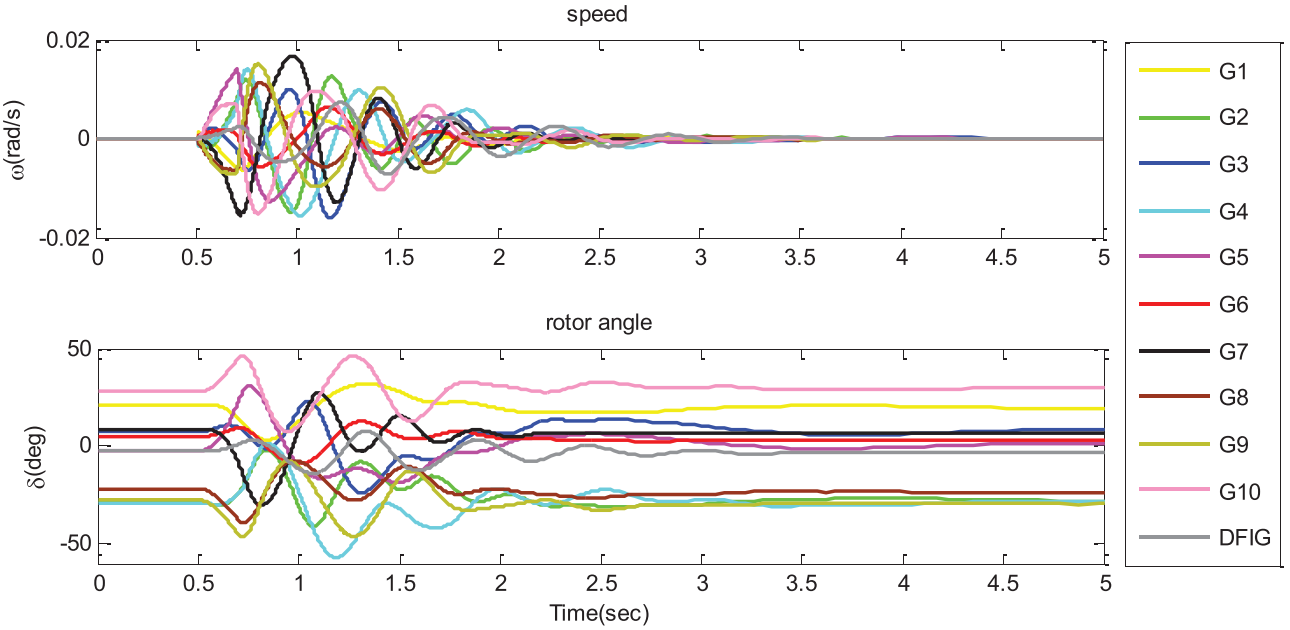

FIGURE 14 The speed and rotor angle of generators 1 to 10 and DFIG

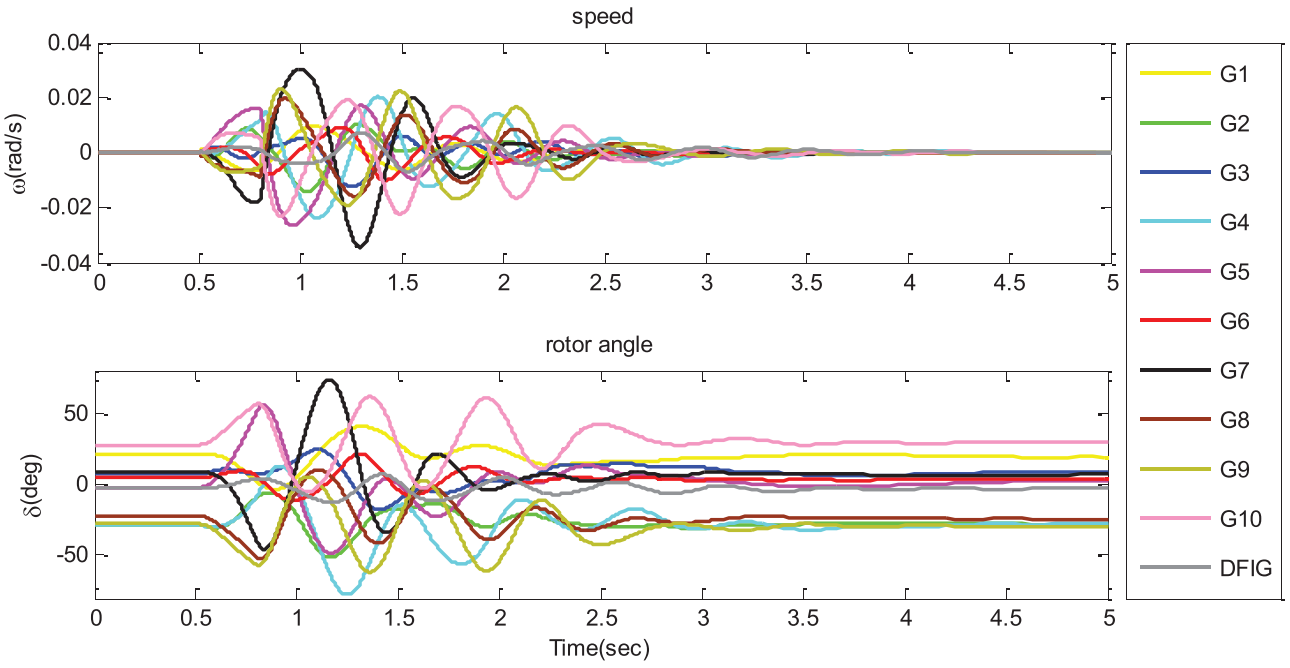

FIGURE 15 The speed and rotor angle of the generators in which the load in bus 12 is increased by about 50% of its base

The simulation results show that the variable time delay value of the control signals has no considerable impact on the proposed control method performance and it is negligible. Figure 8 shows the phase plan of the novel control method for a variable time that is considered in a range of [0,20] ms. In practice, the control signals' time delay is much less than this value. As can be seen, with a variable time delay the system is still stable.

5.2 | Multi-machine

5.2.1 | IEEE 9-bus test system

The first selected multi-machine test system is an IEEE 9-bus that is indicated in Figure 9. This test case contains three generators at buses 1 to 3, three transformers, six lines, and three

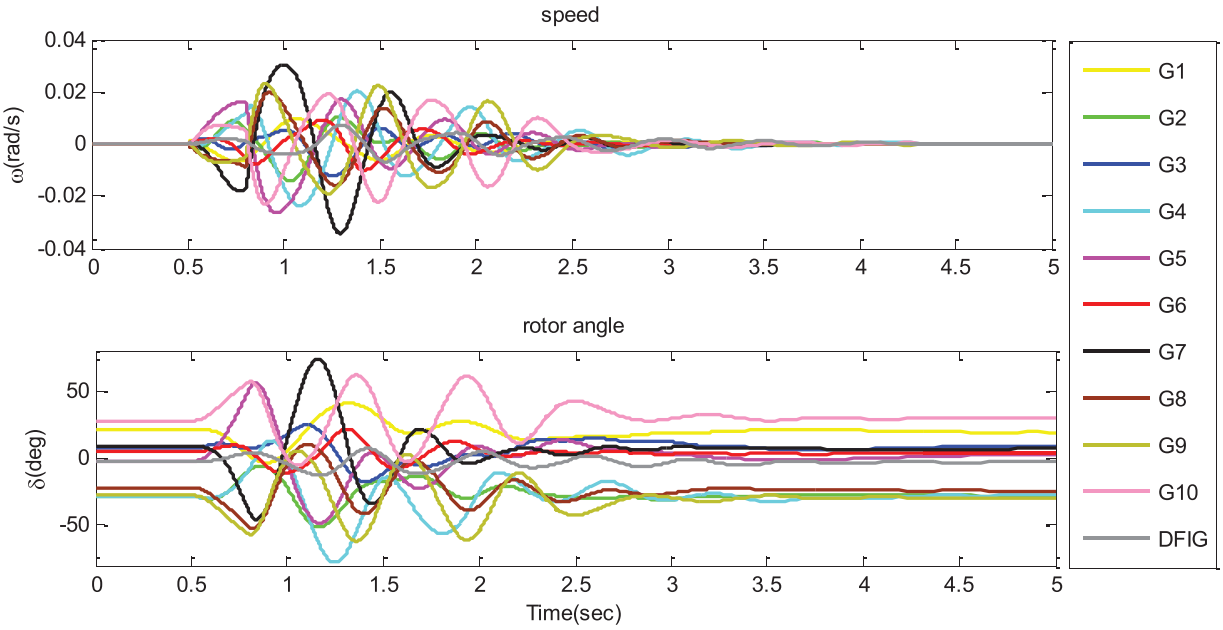

FIGURE 16 The speed and rotor angle of the generators with a 300 ms three-phase short circuit

loads [37]. This system is modified with the addition of a UPFC and DFIG. The UPFC is placed on the line betwixt buses 7 and 8. Also, DFIG is modeled by a compacted wind farm with a capacity of 100 MW (20 units with a capacity of 5 MW each) that is placed at bus 8 [38].

For the above multi-machine system, a three-phase fault happens at the end of line 4–5 (near bus 5). The value of CCT for the uncompensated multi-machine system is equal to 0.134. Table 2 presents CCT results for the different controllers and faults.

The large three-phase disturbances considered in this design are equal to 0.2 s which is happens at 0.5 s and is removed at 0.7 s. According to Figures 10 and 11, the novel control method helps to increase transient stability and damping of oscillation in comparison with the POD control [39] and backstepping control [40], especially in the first swing.

To specify the fluctuation amount and the rate of convergence, and a better comparison of the controllers, the phase plan of the novel control method, the POD control, and backstepping control for SG. 1 is indicated in Figure 12. This figure indicates that the novel control method converges more quickly to the origin, but the POD control and backstepping control balance the system with more time after multiple fluctuations.

5.2.2 | New England Standard 39-bus test system

The second selected multi-machine test system is a New England Standard 39-bus system that has 10-generators that is well known as the 10-machine New-England Power System [41]. SG. 1 represents the aggregation of a large number of generators. Figure 13 shows the single-line diagram of the system. A UPFC is installed between 6 and 7 buses in the system and a DFIG is connected to bus 19 with a short line.

TABLE 3 CCT for different controls and faults in the New England Standard 39-bus test system

	CCT (ms) for different controls			
Fault line	**Without**	**POD**	**Backstepping**	**Novel**
3-4	207	244	251	268
15-16	212	249	256	273

For a New England Standard 39-bus test system, a three-phase fault happens on the line between buses 3 and 4 (near bus 3). The value of CCT for the uncompensated multi-machine system is equal to 0.207. Table 3 presents CCT results for the different controllers and faults.

The large three-phase disturbances considered in this design are equal to 0.2 s which is happens at 0.5 s and is removed at 0.7 s According to Figure 14, the novel control method helps to increase transient stability and damping of oscillation in the first swing.

In Figure 15, the load in bus 12 is increased by about 50% of its base value which shows the robustness properties of the proposed controller against variations in the system topology.

The other large disturbance considered in this study is 300 ms three-phase short-circuit faults. The comparative results for the 300 ms three-phase short circuit are reported in Figure 16.

6 | CONCLUSION

In this paper, a novel non-linear control method TEF-based has been suggested for the transient stability enhancement in

the power systems which consist of SG, DFIG, and UPFC. The novel non-linear controller includes an initial control schemed by TEF and the supplementary damping control extended by second-order sliding mode. The derivative of the control parameters in the novel non-linear controller for DFIG and UPFC were estimated by improved second-order sliding mode observers. The results of simulation in the TMIB and multi-machine (IEEE 9-bus and the New England Standard 39-bus) indicate that the novel non-linear control increases the transient stability under severe disturbances. For the TMIB, IEEE 9-bus, and the New England Standard 39-bus systems the novel non-linear control has grown the CCT by about 23%, 31%, and 29%, respectively, compared to the un-compensated system. Also, the proposed non-linear controller increased CCT and margin of stability by about 7% and 9%, respectively, versus the back-stepping and POD controller. Another outcome of this study is the robustness properties of novel non-linear control versus system topology changes and variable time delay of the control signals.

CONFLICT OF INTEREST

The authors declare that they have no known competing financial conflict of interests or personal relationships that could have appeared to influence the work reported in this paper.

REFERENCES

1. Harish, V.S.K.V., Sant, A.V.: Grid Integration of Wind Energy Conversion Systems. Springer Nature, Switzerland(2020)
2. Ackermann, T.: Wind Power in Power Systems, 2nd ed. Wiley, Hoboken, NJ (2012)
3. Hingorani, N.G., Gyugyi, L.: Understanding FACTS, Concepts and Technology of Flexible AC Transmission Systems. IEEE Press, Piscataway (2000)
4. Kr Dwivedi, A., Vadhera, S.: Reactive Power Sustainability and Voltage Stability with Different FACTS Devices Using PSAT. IEEE SPIN, (2019)
5. Akpeke, N., Muriithi, E., Christopher, M., Mwaniki, C.: Contribution of FACTS devices to the transient stability improvement of a power system integrated with a pmsg-based wind turbine. Eng. Tech. Appl. Sci. Res. 9(6), 4893–4900 (2019)
6. Pal, B., Rehtanz, C., Zhang, X.-P., Flexible AC Transmission Systems: Modelling and Control. Springer, New-York (2006)
7. Maity, S., Ramya, R.: A comprehensive review of damping of low frequency oscillations in power systems. Int. J. Innovative Technol. Exploring Eng. 8, 2278–3075 (2019)
8. Mohandes, B., Abdelmagid, Y.L., Boiko, I.: Development of PSS tuning rules using multi-objective optimization. Int. J. Electr. Power Energy Syst. 100, 449–462 (2018)
9. Shafiullah, M., JuelRana, M., Sh. Shahriar, M., Zahir, M.H.: Low-frequency oscillation damping in the electric network through the optimal design of UPFC coordinated PSS employing MGGP. Measurement 138, 118–131 (2019)
10. Raajeshwar, E., Jeevanandham, A.: Improving Transient Stability of Power System Using UPFC with PID and POD Controllers, IEEE, Piscataway (2017)
11. Chowdhury, M.S.R., Howlader, M.d.M., Kamrul Hasan, A.K.M., Ferdaus, M.R.: Distinctive study of UPFC and fault analysis under simulated environment. In: 2015 Third International Conference on Technological Advances in Electrical, Electronics and Computer Engineering. IEEE, Piscataway (2015)
12. He, P., Arefifar, S.A., Li, C., Wen, F.Y.J., Tao, Y.: Enhancing oscillation damping in an interconnected power system with integrated wind farms using unified power flow controller. Energies 12(2), 322 (2019)
13. Chalice, R., Gabriel, U.: A structure-preserving energy function for a static series synchronous compensator. IEEE Rans. Power Syst. 19(3), 1501–1507 (2004)
14. Nogal, Ł., Robak, S., Machowski, J.: Control algorithm for UPFC based on non-linear model of power system. Electr. Power Comp. Syst. 47, 605–618 (2019)
15. Pakdel, M., Eliasi, H., Ebadian, M.: Dynamic sliding mode control for power flow control with UPFC. In: Iranian Conference on Electrical Engineering (ICEE). IEEE, Piscataway (2018)
16. Azbe, V., Gabrijel, U., Povh, D., Mihalic, R.: The energy function of a general multi-machine system with a unified power flow controller. IEEE Trans. Power Systems 20(3), 1478–1485 (2005)
17. Padiyar, K.R.: Structure Preserving Energy Functions in Power Systems: Theory and Applications. CRC Press, Boca Raton (2018)
18. Yousefian, R., Bhattarai, R., Kamalasadan, S.: Transient stability enhancement of power grid with integrated wide area control of wind farms and synchronous generators. IEEE Trans. Power Syst. 32(6), 4818–4831 (2017)
19. Ghosh, S., Kamalasadan, S.: An energy function-based optimal control strategy for output stabilization of integrated DFIG-flywheel energy storage system. IEEE Trans. on Smart Grid. 8(4), 1922–1931 (2017)
20. Elkington, K., Knazkins, V., Ghandhari, M.: On the stability of power systems containing doubly fed induction generator-based generation. Electr. Power Syst. Res. 78(9), 1477–1484 (2008)
21. Azbe, V., Mihalic, R.: Transient stability of a large doubly-fed induction machine in a pumped-storage plant. Electr. Power Syst. Res. 142, 29–35 (2017)
22. Ghosh, S., Kamalasadan, S.: An energy function-based optimal control strategy for output stabilization of integrated DFIG-flywheel energy storage system. IEEE Trans. Smart Grid 8(4), 1922–1931 (2017)
23. Routray, S.K., Patnaik, R.K., Dash, P.K.: Adaptive non-linear control of UPFC for stability enhancement in a multimachine power system operating with a DFIG based wind farm. Asian J. Control 19(4), 1575–1594 (2017)
24. Kanchanaharuthai, A., Chankong, V., Loparo, K.A.: Transient stability and voltage regulation in multimachine power systems vis-à-vis STATCOM and battery energy storage. IEEE Trans. Power Syst. 30(5), 2404–2416 (2014)
25. Tsai, H.C., Chu, C.C.: Supplementary damping control synthesis: A forward neural networks approximated energy function. In: IEEE Industry Applications Society Annual Meeting (IAS), pp. 23–27. IEEE, Piscataway (2018)
26. Tsai, H.C., Liu, J.H., Chu, C.C.: Integrations of neural networks and transient energy functions for designing supplementary damping control of UPFC. IEEE Trans. Ind. Appl. 55(6), 6438–6450 (2019)
27. Kamel, S., Ibrahim, Y., Rashad, A., Nasrat, L.S., Ahmed, M.H.: Performance enhancement of wind farms integrated with UPFC using adaptive neuro-fuzzy inference system. In: 2019 International Conference on Computer, Control, Electrical, and Electronics Engineering. IEEE, Piscataway (2019)
28. Parvathy, S., Thampatty, K.C.S., Nambiar, T.N.P.: Design and implementation of partial feedback linearization controller for unified power flow controller. Electr. Power Syst. Res. 187, 106438 (2020)
29. Dimitrovska, T., Kopse, D., Azbe, V., Rudež, U., Mihalic, R.: Simultaneous multiple-parameter control in flexible power systems for its stability enhancement. Int. J. Electr. Power Energy Syst. 110, 434–440 (2019)
30. Ghandhari, M., Andersson, G., Zanetta, A.I., Hiskens: Control Lyapunov functions for controllable series devices. IEEE Trans Power Syst. 16(4), 689–694 (2001)
31. Ghandhari, M., Andersson, G., Pavella, M., Ernst,: A control strategy for controllable series capacitor in electric power systems. Automatica 37, 1575–83 (2001)
32. Xiao, Y., Song, Y.H., Sun, Y.Z.: Power flow control approach to power systems with embedded FACTS devices. IEEE Trans. Power Syst. 17(4), 943–950 (2002)
33. Peter, W.S., Pai, M.A.: Power System Dynamics and Stability. New Jersey, Prentice Hall (1998)

34. Kenne, G., Ahmed-Ali, T., Lamnabhi-Lagarrigue, F., Arzandé, A.: An improved rotor resistance estimator for induction motors adaptive control. Electr. Power Syst. Res. 81, 930–941 (2011)
35. Sidhom, L., Brun, X., Smaoui, M., Bideaux, E., Thomasset, D.: Dynamic gains differentiator for hydraulic system control. J. Dyn. Syst. Meas. Control. 137(4), 041017 (2015)
36. Levant, A.: Robust exact differentiation via sliding mode technique. Automatica 34, 379–84 (1998)
37. Radman, G., Raje, R.S.: Dynamic model for power systems with multiple FACTS controllers. Electric Power Syst. Res. 78, 361–71 (2008)
38. Mitra, A., Chatterjee, D.: Active power control of DFIG-based wind farm for improvement of transient stability of power systems. IEEE Trans. Power Syst. 31(1), 82–93 (2016)
39. Martins, L.F., Araujo, P.B., Fortes, E.V., Macedo, L.H.: Design of the PI–UPFC–POD and PSS damping controllers using an artificial bee colony algorithm. J. Control Autom. Electr. Syst. 28, 762–773 (2017)
40. Roy, T.K., Mahmud, M.A., Oo, A.M.T.: Robust adaptive backstepping excitation controller design for higher-order models of synchronous generators in multimachine power systems. IEEE Trans. Power Syst. 34(1), 40–51 (2019)
41. Hiskens, I.: IEEE PES task force on benchmark systems for stability controls. Technical Report (2013)

How to cite this article: Ghaedi, S., Abazari, S., Arab Markadeh, G.: Novel non-linear control of DFIG and UPFC for transient stability increment of power system. IET Gener. Transm. Distrib. 16, 3799–3813 (2022). https://doi.org/10.1049/gtd2.12546

APPENDIX A

$$\dot{S}_{k(\tilde{\delta})} = \frac{(x_{dk} - x'_{dk})}{\omega_s x'_{dk} T'_{0k}} \frac{V_k cos(\delta_k - \theta_k)}{E'_k} + \frac{V_{r(k-m)} sin(\delta_k - \theta_{r(k-m)})}{E'_k}$$

$$\dot{S}_{k(E')} = -\frac{1}{E'^2_k} \left(\frac{(x_{dk} - x'_{dk})}{\omega_s x'_{dk} T'_{0k}} V_k sin(\delta_k - \theta_k) - V_{r(k-m)} cos(\delta_k - \theta_{r(k-m)}) \right)$$

$$\dot{S}_{k(V)} = \frac{(x_{dk} - x'_{dk})}{\omega_s x'_{dk} T'_{0k} E'_k} sin(\delta_k - \theta_k)$$

$$\dot{S}_{k(\tilde{\theta})} = -\frac{(x_{dk} - x'_{dk})}{\omega_s x'_{dk} T'_{0k} E'_k} V_k cos(\delta_k - \theta_k)$$

APPENDIX B
Parameters of the TMIB system

Parameter	SG	DFIG
H(s)	3.12	4.24
T_{do} (s)	6.55	5.44
X_d (p.u.)	1.035	0.987
X'_d (p.u.)	0.296	0.458
X_q (p.u.)	0.474	0.528

APPENDIX C
Parameters of UPFC

Parameter	Series converter	Shunt converter
L(p.u.)	0.16	**0.22**
R(p.u.)	0.005	**0.007**